Subsidence in the Nocturnal Boundary Layer

MERRILEE A. CARLSON* AND ROLAND B. STULL

Boundary Layer Research Team, Department of Meteorology, University of Wisconsin, Madison, WI 53706

(Manuscript received 27 June 1985, in final form 14 December 1985)

ABSTRACT

Nights with clear skies and strong radiative cooling that favor the formation of statically stable nocturnal boundary layers (NBL) are also those nights most likely to have subsidence, because of the presence of synoptic high-pressure regions. The divergence associated with subsidence laterally removes some of the chilled nocturnal boundary layer air causing the NBL to not grow as rapidly as would otherwise be expected. An equivalent interpretation is that subsidence-induced heating partially counteracts the radiative and turbulent cooling.

A new form of nocturnal integral depth scale, H_T, is introduced that incorporates the heating and cooling contributions at night. This scale can be used with a variety of idealized temperature profile shapes, including slab, linear, and exponential. It is shown that observed values of subsidence for two case studies can reduce the NBL growth rate, as measured by $\partial H_T/\partial t$, by 5 to 50% and can cause corresponding errors in the estimation of accumulated cooling unless there is a proper accounting of subsidence.

Subsidence plays a very minor role close to the ground, but for the case studies presented here its heating rate increases with height and becomes of comparable magnitude to the cooling rates of turbulence and radiation within the top third of the NBL. Although no adequate measurements of horizontal advective effects were available for the case studies used here, it appears from an energy balance that advection must not be neglected because its magnitude can be as large as turbulence and radiation.

1. Introduction

Transport processes that govern nocturnal boundary layer (NBL) evolution are radiation, turbulence, subsidence, and horizontal advection. The influences of radiation and turbulence have been well documented by Garratt and Brost (1981), André and Mahrt (1982), Stull (1983c) and Estournel et al. (1985). Since cloud-free, fair-weather nights with strong radiative cooling are often associated with synoptic high pressure, one would expect that subsidence and the corresponding boundary layer divergence are also important. Shaller and Wichmann (1985) have presented field experiment evidence that all four transport processes can significantly affect NBL evolution.

Field experiment analysis, theory, and numerical modeling are combined here to examine the role of subsidence on NBL evolution. In earlier work (Stull, 1983a,b,c) it was suggested that an integral length scale could be defined that is related to the accumulated cooling during the night. Such a definition alleviated a problem associated with locating the top of the statically stable NBL, which is often poorly defined because of its gradual blending into the adiabatic residual layer aloft. However, the assumption of accumulated cooling into the NBL "reservoir" is valid only if there is no loss of air from the reservoir—an assumption that is clearly violated in the case of divergence. Hence, it is believed that the empirical constant a in the equation (Stull, 1983a) for the exponential shape of the NBL potential temperature profile is probably in error, because it is based on a comparison between the area under the temperature curve and the surface heat flux integral for the Wangara and Koorin field experiments, with no accounting of subsidence.

A fresh approach to the integral depth scale concept is taken in this paper. Although we still believe that the integral scale concept is a useful way to model NBL characteristics, we define a new integral depth scale in section 2 that explicitly includes the effects of turbulence, radiation, and subsidence. This differs from the old definition, which explicitly included only turbulence, and implicitly parameterized radiative effects via the parameter a. A theory for the rate of loss of chilled air due to subsidence is also applied to the new depth scale in this section. In section 3, the magnitudes of subsidence and divergence for two case studies from the 1983 Boundary Layer Experiment are presented. Modeling is used in section 4 to ascertain the impact of subsidence on the shape of the temperature profile, both in the NBL and in the overlying residual layer.

2. Theory

The nighttime boundary layer will be idealized to consist of a statically stable NBL underlying an adiabatic residual layer. The residual layer starts with an

* Present affiliation: Department of Environmental Protection, State House, Station 17, Augusta, ME.

adiabatic lapse rate because it is formed in the evening as the turbulence in the convective mixed layer decays (Stull, 1983c). Turbulent and radiative cooling near the earth's surface at night then chills the bottom portion of the residual layer, creating the two-layer structure in this idealization. Although it will be shown later in the modeling part of this study that direct radiative cooling of the residual layer can modify its lapse rate, we will initially assume a simpler case here such that the adiabatic lapse rate in the residual layer is preserved during any such cooling.

a. Effect of subsidence

As the NBL grows, divergence laterally removes some of the chilled air from the NBL, and the associated subsidence brings down warmer residual-layer air to take its place (Fig. 1). Subsidence/divergence affects the heat budget of the NBL only as long as the NBL is cooler than the residual layer. If there is no chilled air in the NBL such as occurs at approximately sunset, then subsidence can cause no change of temperature because of the adiabatic lapse rate in the residual layer.

To quantify this effect, start with the heat budget relationship given by the heat-flux-history length scale: $H(t) = I[Q_H(\tau)]/\Delta\theta_s(t)$, where Q_H is the surface heat flux in kinematic units (e.g., K m s^{-1}), $\Delta\theta_s$ the potential temperature difference between air near the surface and the residual layer air,

$$I[\ \ ] = \int_0^t [\ \ ]d\tau,$$

t is the time since evening transition to cooling at the surface, and τ is a dummy of integration (Stull, 1983a,b,c). When this heat budget is rearranged to the form $(H\Delta\theta_s) = I[Q_H(\tau)]$ and differentiated with respect to time, the following rate equation is obtained: $d(H\Delta\theta_s)/dt = Q_H(t)$. We note that the heat flux-history length scale is defined solely in terms of turbulent heat flux from the surface.

Although it was shown (Stull, 1983b,c) how radiative effects could be modeled without changing the definition of H, it is apparent in the present study that a more convenient definition of length scale could be defined to directly include all forcings on the heat budget, such as turbulence, radiation, and subsidence. Define a "total integral length scale," H_T, by

$$d(H_T\Delta\theta_s)/dt = Q_H(t) + Q_R(t) + Q_S(t), \qquad (1)$$

where Q_R is the radiative heat flux difference across the NBL that is in excess of the difference measured in the residual layer, and Q_S is the effective heat flux associated with subsidence. If the upward radiative flux, R, is defined by $R = R_0 + R_*$ (Stull, 1983c), where the background radiative flux R_0 acts both in the NBL and the residual layer and surface-induced radiation R_* acts only in the NBL, then we see that

$$Q_R = R_*|_{\text{top}} - R_*|_{\text{bottom}},$$

where top and bottom refer to the NBL. At night Q_R, Q_H, and $\Delta\theta_s$ are usually negative.

Of more interest here is an expression for Q_S. If NBL air has a bulk heat deficit of $H_T\Delta\theta_s$ compared with a neutral boundary layer, and if air diverging out of a boundary layer carries its heat deficit along with it, then the net effective flux associated with divergence β is

$$Q_S = -\beta H_T\Delta\theta_s. \qquad (2)$$

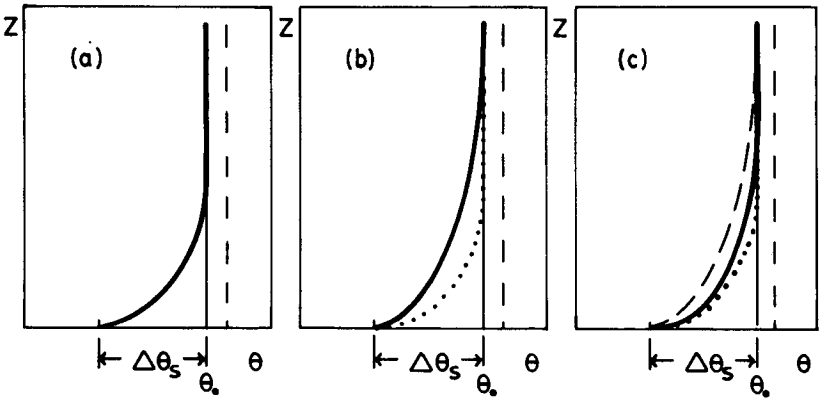

FIG. 1. Schematic drawings showing the modification of a nocturnal stable layer growth by subsidence. The initial potential temperature sounding [solid line in (a), dotted line in (b) and (c)] grows by turbulent, radiative, and possibly advective processes in the absence of subsidence [solid line in (b), curved dashed line in (c)]. Subsidence, however, causes the growth to be slower, as indicated by the solid line in (c). The vertical dashed lines indicated the initial mixed-layer potential temperature at the start of the evening. The vertical line labeled θ_0 indicates the reference sounding as modified from the earlier mixed layer sounding by uniform, background radiational cooling. The temperature jump at the surface, $\Delta\theta_s$, is also shown.

For the special case of no heat deficit ($H_T\Delta\theta_s = 0$), then (2) states that there will be no heating regardless of the magnitude of subsidence or divergence. (See Fig. 1c.) Again, this is based on the idealization of an adiabatic residual layer above the NBL.

Inserting (2) into (1) and solving this ordinary differential equation yields

$$H_T\Delta\theta_s = \exp[-\beta(t)t]I\{[Q_H(\tau) + Q_R(\tau)]\exp[\beta(\tau)\tau]\}. \quad (3)$$

For the special case of no subsidence, this reduces to $H_T\Delta\theta_s = I[Q_H(\tau) + Q_R(\tau)]$, as expected. The left-hand side of (3) is equal to the area under the potential temperature profile, as shown in Fig. 2c. Hence, it is a measure of the overall degree of development (strength and thickness) of the NBL. The right-hand side, in the absence of subsidence, shows that turbulence and radiation cause the NBL to develop and grow. With subsidence, however, the strength and/or thickness of the NBL will not grow as fast. If the NBL is viewed as a reservoir storing chilled air, then divergence associated with subsidence acts like a leak in the reservoir.

b. *Evolution of NBL shape*

Equation (3) is not based on any statement about the shape of the NBL temperature profile and is thus general enough to be used with any shape, including well-mixed slab (Zeman, 1979), linear (Estournel et al., 1985), polynomial (Yamada, 1979), or exponential (Stull, 1983a). In (3) it was assumed for simplicity that the divergence is constant with height, both in the NBL and in the residual layer. By mass continuity, this necessitates a linear increase in subsidence velocity, w_s, with height: $w_s = -\beta(t)z$. It is shown herein that not only do the slab, linear, and exponential profiles preserve their shape during this subsidence, but that their respective depths after subsidence are a constant fraction, b, of their original (nonsubsidence) depths.

To simplify the examination of shape evolution, picture a situation where the NBL first develops without subsidence. Then switch off the effects of turbulence and radiation and turn on the effects of subsidence. Since potential temperature is conserved during adiabatic descent, subsidence acts to remap each point in the initial profile to a new height (but same potential temperature) in the final profile. Using the classical calculus definition for velocity, dz/dt, in the expression for linear subsidence change with height, and integrating over time period Δt, gives an equation mapping each initial height, z_i, of the sounding into a final height, z_f:

$$z_f = bz_i, \quad (4)$$

where

$$b = \exp\left[-\int_0^{\Delta t}\beta(\tau)d\tau\right].$$

If β is nearly constant over time period Δt, then $b = \exp(-\beta\Delta t)$, where the parameter b is not a function of height.

The slab problem is trivial because its actual depth $h = H_T$, and all lapse rates are adiabatic except for the discontinuity across the top of the NBL. (See Fig. 2a.) As a result, (4) can be used directly to map the nonsubsidence value of H_{Ti} into the value after subsidence, H_{Tf}: $H_{Tf} = bH_{Ti}$. The slab shape is conserved.

For an initial linear profile before subsidence, the bottom coordinates of the sounding on a θ–z plot are given by ($z = 0$, $\theta = \theta_0 + \Delta\theta_s$), where θ_0 is the residual layer potential temperature at time t. Remember that $\Delta\theta_s$ is negative at night, making $\theta < \theta_0$. The top coordinates are given by ($z = h_i$, $\theta = \theta_0$), where $h_i = 2H_{Ti}$ by the first law of thermodynamics (i.e., area under the sounding must equal $H_T\Delta\theta_s$). After subsidence, the linear mapping preserves the linear profile by definition, causing the final height to be given by $h_f = bh_i$, and $H_{Tf} = bH_{Ti}$ as before (see Fig. 2b).

For the exponential shape (Fig. 2c), the temperature

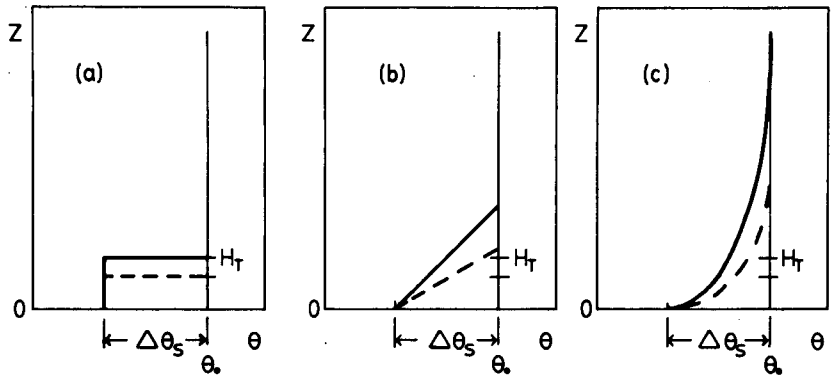

FIG. 2. Examples of the evolution of different potential-temperature profile shapes under the influence of subsidence: (a) slab; (b) linear; (c) exponential. The location of the integral depth scale, H_T, and the near-surface amount of temperature change since transition, $\Delta\theta_s$, are also shown. As in Fig. 1, no other transport mechanisms are assumed to be acting during the sketched evolution, except for subsidence.

difference $\Delta\theta(z)$ between the residual layer and the sounding at any height z is given by

$$\Delta\theta(z) = \Delta\theta_s \exp(-z/H_T). \quad (5)$$

This differs slightly from the expression in Stull (1983a), because the effects of radiation are included in the definition of H_T, instead of being described by an additional factor a. There is no well-defined top to such an exponential sounding, so the definition of $h = 5H_T$ (i.e., where $\Delta\theta = 0.02\Delta\theta_s$) as suggested by Stull (1983a) can be used.

Treating (5) as representing the initial presubsidence sounding ($z = z_i$, $H_T = H_{Ti}$), the mapping caused by subsidence ($z_f = bz_i$) leaves $\Delta\theta(z_f) = \Delta\theta_s \exp[-z_f/(bH_{Ti})]$. Into this expression we can insert the definition that $H_{Tf} = bH_{Ti}$, thereby showing that the exponential shape is preserved after subsidence.

Although the previous examples were performed by integrating over a finite time interval while turbulence and radiation were turned off, it is obvious that these three shapes are conserved even during an infinitesimal time increment. Hence, if turbulence and radiation are assumed to generate any of those three idealized shapes (as was modeled by the investigators listed earlier), then the addition of subsidence acting simultaneously with turbulence and radiation will not alter those respective shapes, although their depths will increase less rapidly.

3. Field experiment

To test the conclusions of section 2 that subsidence can impact the evolution of the NBL, a combination of field experiment and model prediction results are used. The field experiment provides the initial and boundary conditions for the numerical model, where the model is used to isolate the contributions of radiation, turbulence, and subsidence on the overall evolution.

During the 1983 Boundary Layer Experiment (BLX83) in Oklahoma (Stull and Eloranta, 1984), a special subexperiment was conducted near Canton (36°4′48″N, 96°40′48″W, elevation 506 m) to observe NBL evolution. The Canton site was located on a grassy knoll southwest of Canton Reservoir Dam. (See Fig. 3 for a local map.) The location was selected because of access to electrical power and shelters, because of support from the local park service, and because the location on a knoll would remove the instruments from the potential influence of drainage winds. A 35 m tall water tower was located on top of the knoll about 15 m to the north of the instrument site. Some of the power for the experiment came from an electrical connection at the base of the water tower.

Several nights of fair weather were selected for intensive study. Two of those nights, presented here as cases A and B, were characterized by predominantly light southerly winds without complicating advective effects from the lake. The other nights were excluded because of instrument failures, advection from the north over the reservoir, or interference by clouds. Case A is the night of 15–16 June 1983, for which soundings were taken at 1400, 2120, 2300, 0300, and 0625 CDT (CDT = GMT − 5). Case B is the night of 18–19 June 1983, with soundings at 1400, 2100, 2230, 0030, 0230, 0430, and 0600 CDT. Figures 4a–d show the synoptic conditions during these periods. In brief, high pressure was centered over Oklahoma during case A, with light southerly breezes (900 mb winds of 7–13 m s^{-1}). For case B, a broad region of high pressure over the southeast United States caused southerly winds of about 13–17 m s^{-1} at 900 mb.

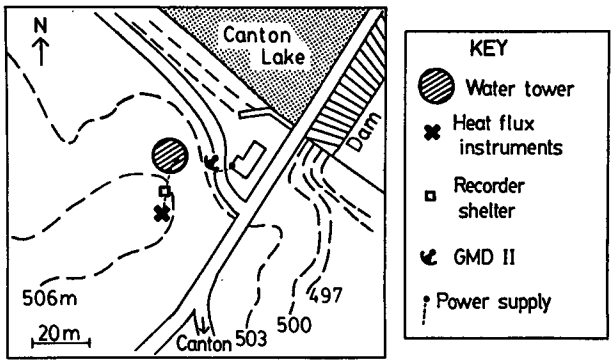

FIG. 3. Topographic map of the Canton Lake rawinsonde launch site in Oklahoma.

Slow ascent Airco rawinsondes were launched to provide soundings of temperature, relative humidity, and pressure. Precision estimates for each sensor are 0.5°C, 5% and 1 mb, respectively, with resolutions of 0.01°C, 1%, and 0.1 mb. The soundings for these two cases are shown in Figs. 5a and 5b. Not only is the growth of the NBL evident, but subsidence can also be seen in the elevated inversions on both days. By measuring the height change of the elevated inversion between successive soundings, (4) can be inverted to solve for the divergence $\beta = \ln[z_i/z_f]/\Delta t$, where $\Delta t = t_f - t_i$ is the time interval between soundings. Figure 6 shows a schematic of this method, and Table 1 gives the resulting estimates of subsidence velocity and divergence rate.

To estimate $\Delta\theta_s$ from these soundings, it is necessary to define the reference temperature θ_0. For the simple idealized situation of section 2, this reference temperature is just the current potential temperature of the adiabatic residual layer. An estimate of this temperature was made by starting with sounding data from the previous day's mixed layer and then forecasting the warming up of the mixed layer and the transition to cooling in the evening. Examination of the soundings in Figs. 5 show that the observed nighttime soundings differ, sometimes appreciably, from this reference temperature. This suggests that advection, which was neglected in the idealized model of the previous section, can be an important element in NBL evolution.

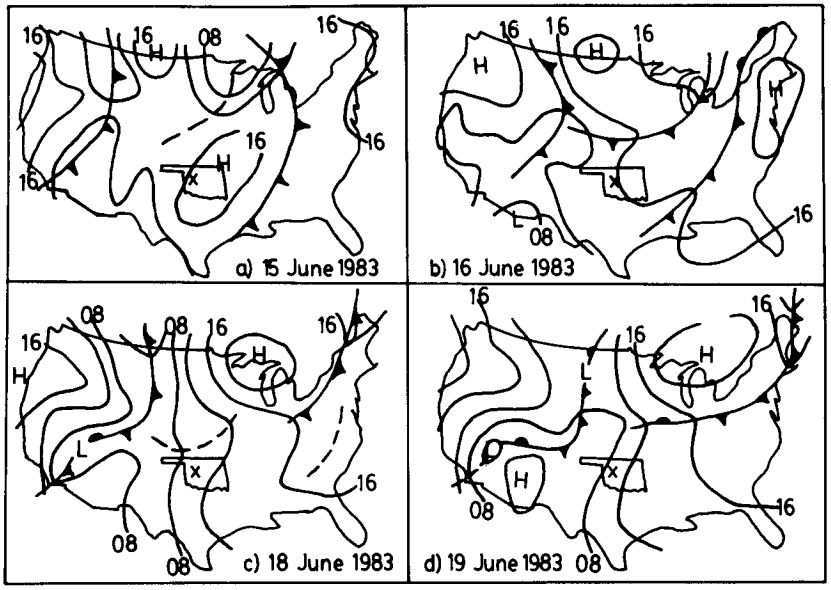

FIG. 4. Surface synoptic weather maps valid at 1500 GMT on the dates shown for case A (Figs. a and b) and for case B (Figs. c and d). The Canton Lake field site location is indicated with the "X."

Case B, in particular, shows that it is virtually impossible to find the reference temperature from the sounding dataset itself, because there is no adiabatic residual layer evident in the soundings. In view of all of these difficulties, estimates of $\Delta\theta_s$ are given in Table 2, where the reference temperatures plotted in Figs. 5a, b were used. Looking at the case B sounding, one can see little or no temperature change at $z = 2000$ m. Although this suggests that advection is relatively small at that height, it still might be larger at lower heights in the NBL.

A shielded net radiometer was used to measure net radiation Q_* and an array of subsurface flux plates and thermocouples were used to estimate the heat flux conducted into the ground Q_G. Heat flux into the air Q_H was then calculated from a simplified surface budget $Q_H = Q_* - Q_G$, where latent heating effects such as dew are neglected. The time evolution of terms in this heat budget are plotted in Fig. 7, where values of Q_H on the order of -50 W m^{-2} are common.

No direct measurements of the radiative heat flux, Q_R, were made during the field experiment, therefore it is by necessity set to zero when used in (3) to calculate an integral length scale. This means that the resulting length scale is not a "total" scale, H_T, as defined by (3), but is closer to the heat-flux-history scale, H, used earlier. Although the neglect of Q_R does not reduce our ability to focus on the effects of subsidence, we recognize that radiation plays an important role in the evolution of the NBL. For this reason, we undertook the modeling studies presented in section 4 to estimate the relative importance of all three factors: radiation, subsidence, and turbulence. The fourth factor, advection, was estimated as a residual.

Knowing β, Q_H, and $\Delta\theta_s$ as a function of time, (3) is used to calculate the integral length scale, H, for two scenarios: 1) no subsidence and 2) subsidence associated with the observed value of β. The results, listed in Table 2, show that subsidence for these cases caused the growth rate of H to be reduced by 5 to 50%.

4. Model simulation

Lacking in the BLX83 measurements are vertical profiles of radiation divergence, subsidence, and turbulence. Therefore, the relative importance of these factors as a function of height cannot be observationally determined. Instead, numerical models were designed to simulate the processes of turbulence, radiation, and subsidence, given the BLX83 observations as initial and boundary conditions. The same two case-study nights are simulated.

Temperature tendency at any height can be split into four parts: contributions from subsidence, radiation, turbulence, and horizontal advection. This may be expressed as

$$\partial T(z)/\partial t|_{\text{total}} = \partial T(z)/\partial t|_{\text{sub}} + \partial T(z)/\partial t|_{\text{rad}} + \partial T(z)/\partial t|_{\text{turb}} + \partial T(z)/\partial t|_{\text{adv}}. \quad (6)$$

A simple one-dimensional boundary layer model is used to evaluate the first three contributions. Each forecast is initialized from an adiabatic mixed-layer sounding: $\theta_0 = 302.4$ K for case A and $= 305.4$ K for case B. A vertical grid increment of 25 mb is used be-

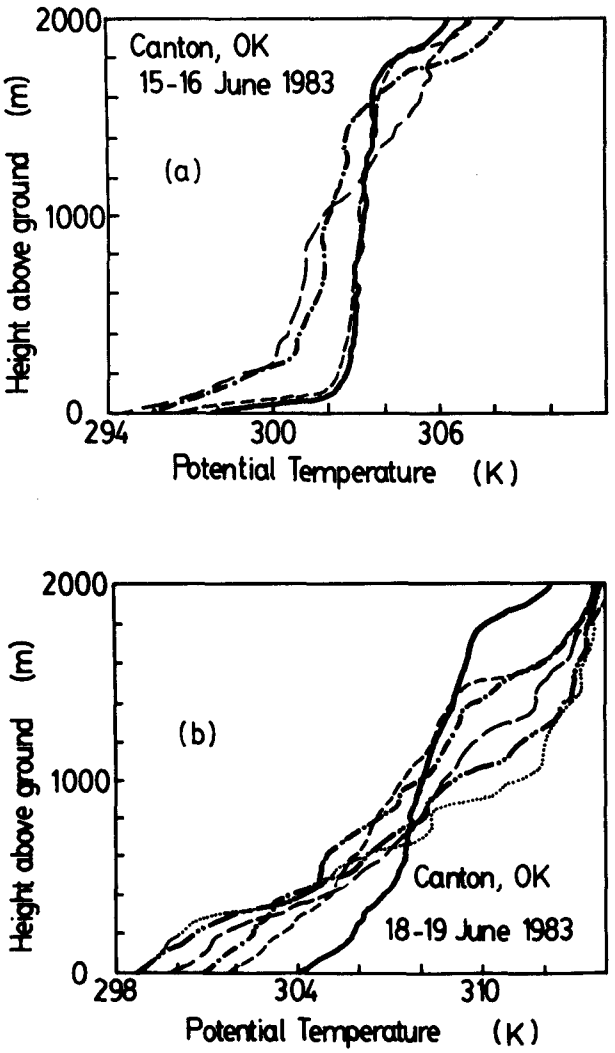

FIG. 5. (a) Potential temperature profiles for case A (15–16 June 1983) at Canton, Oklahoma: (· · · · ·), reference temperature; (——), 2120; (---), 2300; (-·-), 0300; (——), 0625 CDT. (b) Same for case B (18–19 June 1983): (· · · · ·) reference temperature; (——), 2100; (---), 2230; (-·-), 0030; (——), 0230; (-· ·-), 0430; (· · · · ·), 0600 CDT.

tween the surface (about 959 mb) and 700 mb, and a time step of 6 min is taken.

For the subsidence term, the observed lapse rate at any height $[\partial\theta(z)/\partial z]$ and the divergence rate, β, are used to give

$$\partial T(z)/\partial t|_{\text{sub}} = \beta z[\partial\theta(z)/\partial z].$$

There was insufficient BLX83 data to directly evaluate the advective contribution during the two case-study nights; therefore, this term is estimated as a residual between the observed and forecast soundings. One must recognize the limitations using such a residual approach; namely, all of the errors associated with the measurements and modeling are also lumped in with the advection contribution. We estimate the sum of these errors to be no greater than about 1°C d^{-1} for case A and 3°C d^{-1} for case B.

Longwave radiation flux is calculated using the flux-emissivity approach for water vapor emissions, and neglects the smaller carbon dioxide effects (Staley and Jurica, 1970; Stull, 1976, 1983a,b,c). The radiative cooling is then found from a simple flux divergence:

$$\partial T(z)/\partial t|_{\text{rad}} = -\partial F_R/\partial z.$$

Skin temperature at the earth's surface, necessary for the radiative flux calculation, is estimated from the subsurface temperature profile.

Since radiation and subsidence are explicitly parameterized in this model, the turbulence parameterization should not include an additional factor for those processes. Therefore, a simple exponential potential temperature profile is assumed having an e-folding depth of H, where H (sans subsidence) is supplied as a boundary condition from Table 2. Differentiating this profile with respect to time yields

$$\partial T(z)/\partial t|_{\text{turb}} = 0.5Q_H/H[1 + z/H] \exp(-z/H).$$

Initially,

$$\partial T(z)/\partial t|_{\text{turb}}$$

is set to zero until $H > 0$.

During the two fair-weather cases studied here, there was a positive subsidence contribution to the temperature tendency, and negative contributions from ra-

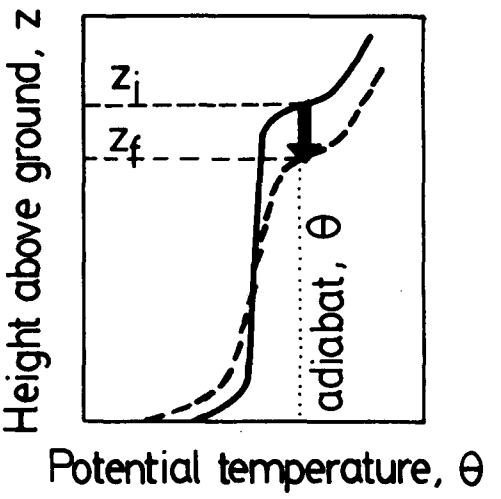

FIG. 6. Diagram showing technique used to estimate subsidence of an elevated inversion. The initial, z_i, and final, z_f, heights of one potential temperature value within an elevated inversion are used. The same process is repeated for a number of adiabats to get a statistically significant sample. Solid line, initial sounding; dashed line, final sounding. The heavy arrow schematically indicates the subsidence motion.

TABLE 1. Estimates of subsidence velocity (w) and divergence (β) based on the measured downward movement (Δz) of elevated temperature inversions (of height z) during time Δt. Data are from rawinsonde soundings made near Canton, Oklahoma, during the BLX83 field experiment, June 1983.

Date (1983)	Time (CDT)	z (m)	Δz (m)	Δt (s)	$-w^*$ (cm s^{-1})	β (10^{-5} s^{-1})
15 June	2119	1711				
			59	6060	1.0	0.58
	2300	1652				
			22	14340	0.2	0.093
16 June	0259	1630				
			267	12300	2.2	1.45
	0624	1363				
						avg 0.71
18 June	2101	1782				
			285	5280	5.4	3.30
	2229	1497				
			99	7260	1.4	0.94
19 June	0030	1398				
			183	7080	2.6	1.98
	0228	1215				
			163	7380	2.2	1.95
	0431	1052				
			156	5220	3.0	3.08
	0558	896				
						avg 2.25

* Subsidence errors are ±0.75 cm s^{-1}, based on a temperature sounding uncertainty of ±0.5°C. Additional subsidence uncertainty is associated with the inability to distinguish between subsidence and advective changes in the temperature structure of the soundings.

diation and turbulence. Advection is inferred to have contributed to warming in the top portion of most of the soundings, but caused cooling in the bottom portions.

Each case study is broken into several periods, where each period is bracketed by rawinsonde soundings. The left portion of each figure (Figs. 8 and 9) shows the evening reference sounding, the observed sounding at the start of the time period, and both the forecast and observed soundings at the end of the period. The forecast sounding at the end of each period is based on an initial condition equal to the observed sounding at the start of the period, except for the first period, which is started from the calculated evening reference sounding.

The right portion of these figures shows the tendency terms of (6). During each period, some of the tendency terms changed dramatically. Therefore, the tendencies at the beginning and end of each period are plotted, instead of showing the average tendency of each term over the period. For the residual (advection) term, only one curve is drawn to indicate the difference between the observed and forecast soundings at the end of each period.

TABLE 2. Near-surface air pressure and temperature are shown as a function of time during the two BLX83 case-study nights. The magnitude of air temperature change near the surface since evening transition is also given ($\Delta\theta_s$). Calculations of the integral length scale H both with [Eq. (3)] and without subsidence are tabulated.

Date (1983)	Time from transition (hr)	Surface pressure (mb)	Surface air temp (C)	$-\Delta\theta_s$ (C)	H	
					No subsidence (m)	With subsidence (m)
15 June	0.0	958.9	29.2	0.0		
	2.1	959.5	20.71	8.53	40	38
	3.8	956.9	19.86	9.38	104	66
16 June	7.8	956.7	18.72	10.52	119	108
	11.3	957.1	17.47	11.77	122	83
18 June	0.0	951.1	32.2	0.0		
	1.9	950.5	26.47	5.77	39	37
	3.4	951.0	24.12	8.12	56	47
19 June	5.4	952.2	23.37	8.87	87	88
	7.4	951.9	22.38	9.86	110	85
	9.4	950.4	21.21	11.03	131	97
	11.3	950.7	21.53	10.71	159	80

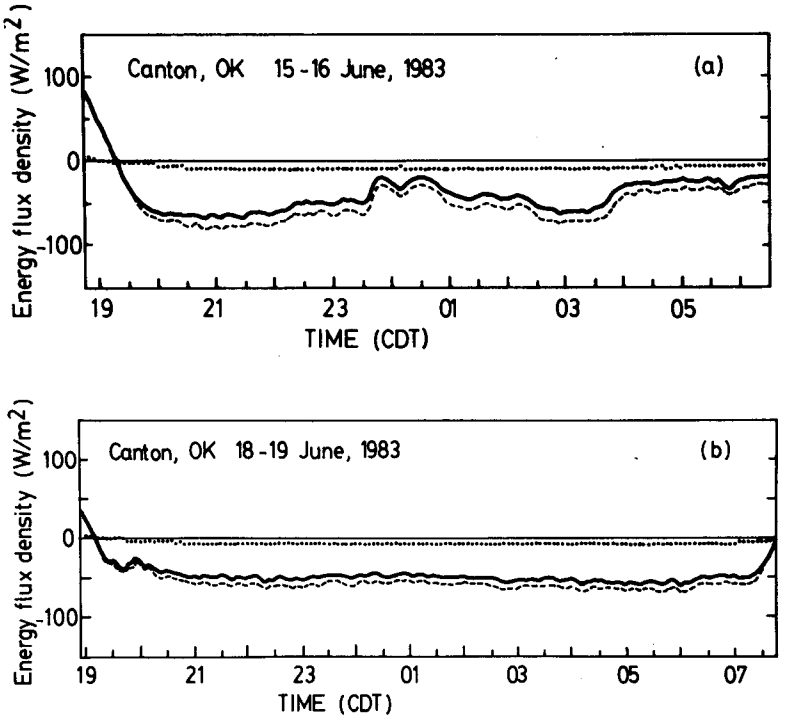

FIG. 7. Net incoming radiation (dashed line) and heat flux down into the ground (dotted line) are combined to yield the heat flux up into the air (solid line) as a function of time during the two case-study nights at Canton. (a) 15–16 June 1983 and (b) 18–19 June 1983.

Figures 8a–d show the time evolution of these contributions as a function of height for case A. Radiative effects are roughly constant with height, contributing about 2°C d^{-1} to the total cooling rate in agreement with André and Mahrt (1982) and Garratt and Brost (1981). A closer look, however, reveals that there is slightly more cooling in the bottom part of the residual layer than in the top part, thereby creating a slightly statically stable lapse rate. Turbulence causes the largest amount of cooling near the surface; its contribution decreases rapidly with height for this case. In particular, turbulence contributes over 50°C d^{-1} to the cooling rate near the ground at the start of the night, but this contribution reduces to about 10°C d^{-1} by the end of the night. Thus, the combined effects of turbulence and radiation are to create a statically stable lapse rate, both in the NBL and in the overlying residual layer.

Subsidence, by definition, always causes zero warming at the earth's surface because the subsidence velocity is zero there, but it can cause large rates of warming above the surface if the ambient lapse rate is statically stable. Initially, however, there is zero warming by subsidence because the evening lapse rate is adiabatic, as determined by the previous day's mixed layer. As is obvious in Fig. 5a, the residual layer for this case changes from adiabatic to statically stable, perhaps because of the influence of radiative cooling. Once it is statically stable, subsidence strengthens the stability and causes increased warming. Figure 8d shows that by the end of the night, subsidence warming of about 3°C d^{-1} is greater than radiative effects at all heights and greater than turbulence effects in the top quarter of the NBL.

The residual (advection) contributes as much as 10°C d^{-1} warming in the top portion of each sounding. Initially in the evening, there is very little advective cooling at the surface (Fig. 8a). As the night progresses, however, advective processes cool an increasingly thick layer near the bottom of the NBL. This low-level phenomena might be associated with a 12–13 m s^{-1} nocturnal jet centered at about 900–930 mb, with a wind direction from 170–200°.

Figures 9a–f show the time evolution for case B. Although turbulence and radiation are of similar magnitudes to those of case A, the subsidence term is much larger. The primary reason for this is that the observed soundings became strongly statically stable during the night. This stability, coupled with the strong subsidence velocities, created warming rates up to 10°C d^{-1} in the residual layer and top of the NBL. Larger warming rates were observed above the residual layer in association with the subsidence of an elevated temperature inversion.

By comparing the forecast vs the observed soundings in the left portion of Figs. 9a–f, it is obvious that radiation, subsidence, and turbulence are insufficient to explain the observed evolution. The residual (advection) for this case was very large, with magnitudes of 20–35°C d^{-1} warming in the top of the sounding and

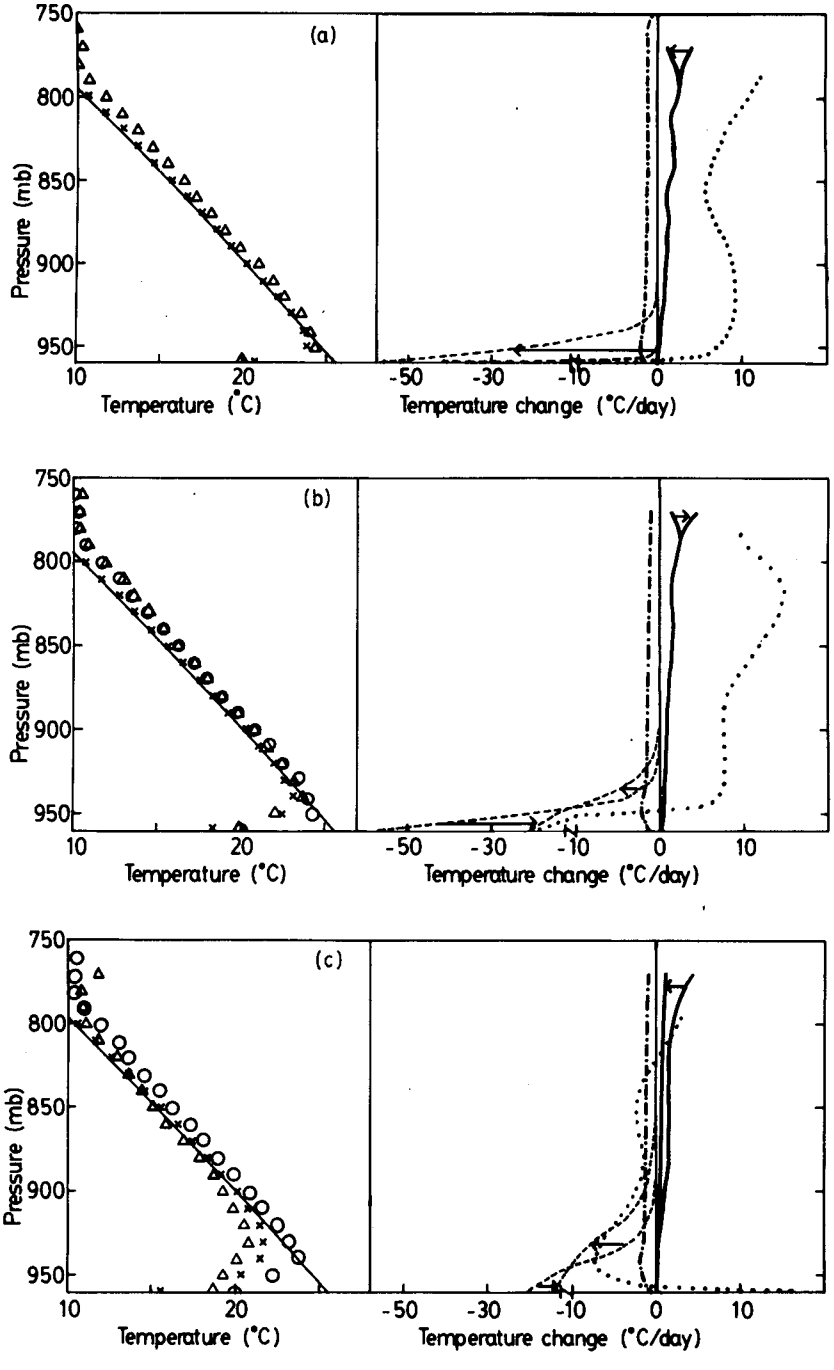

FIG. 8. Left panel shows the temperature profiles for case A, the night of 15–16 June 1983 case at Canton, Oklahoma: solid line, reference temperature; (×), forecast valid at the end of the period; (○), observation valid at the beginning of the period [equal to the reference temperature for (a)]; and (△) the verification (observation) valid at the end of the period. Right panel shows the cooling rate contributions due to turbulence (dashed line) at both the beginning and end of the period; radiation (dashed–dotted line) during the period; subsidence (solid line) both at the beginning and end; and the residual (dotted line) (interpreted as advection) between forecast and verification. The arrows indicate the change in cooling rate between the beginning and end. Periods: (a) 1900–2120, (b) 2120–2300, (c) 2300–0300, and (d) 0300–0625 CDT.

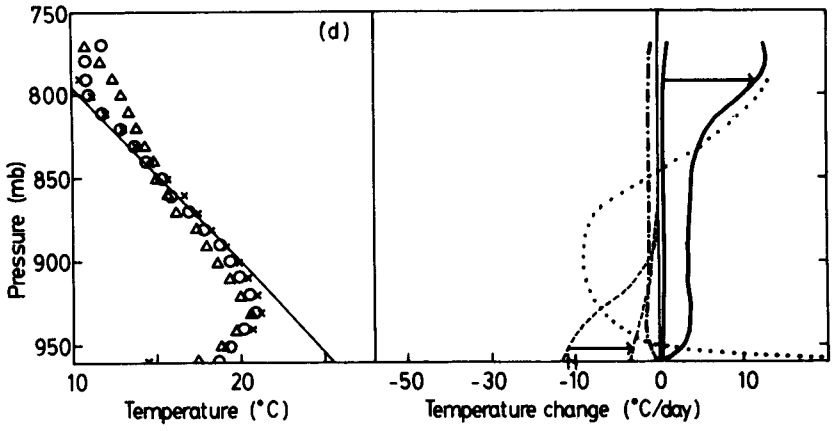

FIG. 8. (*Continued*)

30–50°C d^{-1} cooling in the bottom portion. The nocturnal jet on this night was very strong, with 20–21 m s^{-1} winds from 160–200° at a pressure of 890–910 mb.

Also, the exponential cooling rate profile assumed for the turbulence term appears to be adequate for case A, but inadequate for case B. In particular, case B exhibits more of a linear profile, such as suggested by Estournel et al. (1985). For both cases, it is clear that subsidence can be just as important as turbulence and radiation, particularly in the top quarter of the NBL. In the residual layer, subsidence warming can be large enough to counteract much of the radiative cooling. For both cases, the residual term (advection) accounts for warming in the residual layer, but indicates increased cooling throughout most of the NBL. In an advective situation such as this with light surface winds and a stronger jet aloft, internal boundary layer formation may cloud the interpretation of the residual term.

5. Summary and conclusions

Nights with clear skies and strong radiative cooling favorable for the formation of nocturnal boundary layers are also those nights most likely to have subsidence. In the high pressure regions with light winds, subsidence is, in part, responsible for the reduction in cloud cover. Thus, we should expect radiative cooling and subsidence to go hand in hand for nonadvective situations.

In this paper, two cases were shown to demonstrate the importance of subsidence. Both cases, fair weather nights during June 1983, were part of the 1983 Boundary Layer Experiment. By utilizing slow ascent rawinsonde soundings, radiometers, and ground flux sensors, the contributions to total cooling rate by turbulence, radiation, and subsidence were estimated. It was found that

a) In the bottom third of the NBL, turbulence usually dominates over both radiation and subsidence.

b) In the top third of the NBL, all three terms can be of equal magnitude.

c) Higher (in the residual layer) subsidence-induced warming rates of 1° to 10°C d^{-1} are possible once radiation or advection first stabilizes the residual layer.

d) Horizontal advection, although estimated as a residual in these case studies, can be more important than radiation or subsidence and should not be neglected.

For these case studies, subsidence was estimated by observing the lowering of elevated (non-NBL) temperature inversions. Subsidence velocities of 0.2 to 5.4 cm s^{-1} at the height of this inversion were estimated, leading to divergence values of $\beta = 0.09 \times 10^{-5}$ to 3.3×10^{-5} s^{-1}.

A theory is presented (3) demonstrating the reduction in depth of the NBL by subsidence. This theory is independent of the assumed shape of the temperature profile. It does employ the concept of an integral length scale (1) that is a measure of the accumulated cooling that has occurred since the evening transition to negative heat flux at the surface. This new integral length scale, H_T, includes the effects of turbulence, radiation, and subsidence, instead of just using turbulence as was proposed earlier (Stull, 1983a,b,c). It is shown how such an integral length scale is compatible with a variety of temperature profile shapes, thereby allowing us to use a forecast equation for just one height scale, H_T, instead of a variety of NBL height definitions.

Although this study was initiated in part to demonstrate the value of the exponential-shaped parameterization for the NBL potential temperature profile, we eventually proved to ourselves that there is no one unique shape. Instead, it became obvious that shapes range from exponential, through linear, to slab-like nocturnal mixed layers depending on the history of forcings acting on the NBL. In future research, we plan to classify the observed temperature profile shapes according to the forcings acting on the NBL.

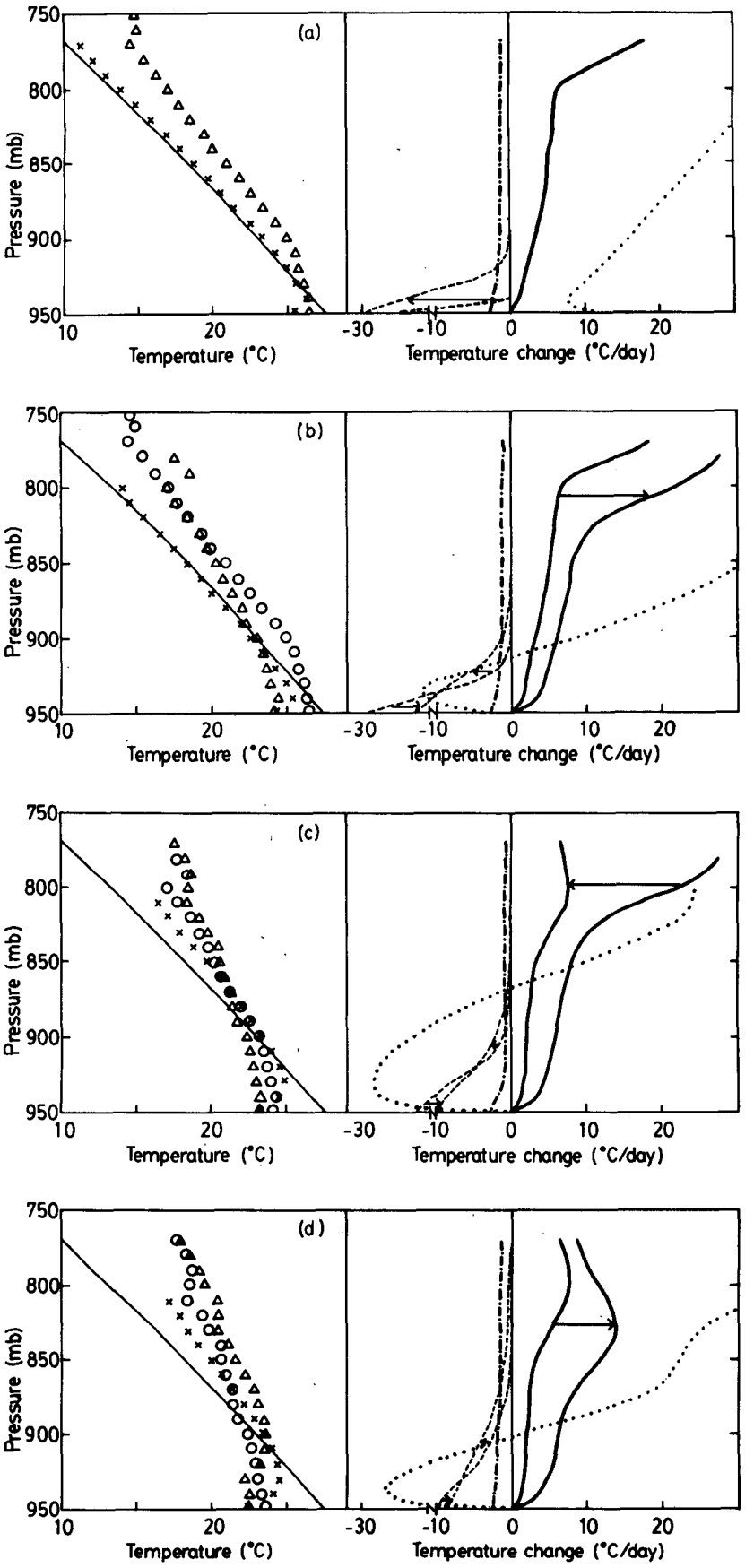

FIG. 9. As in Fig. 8 except for case B: 18–19 June 1983. Periods are (a) 1900–2100, (b) 2100–2230, (c) 2230–0030, (d) 0030–0230, (e) 0230–0430, and (f) 0430–0600 CDT.

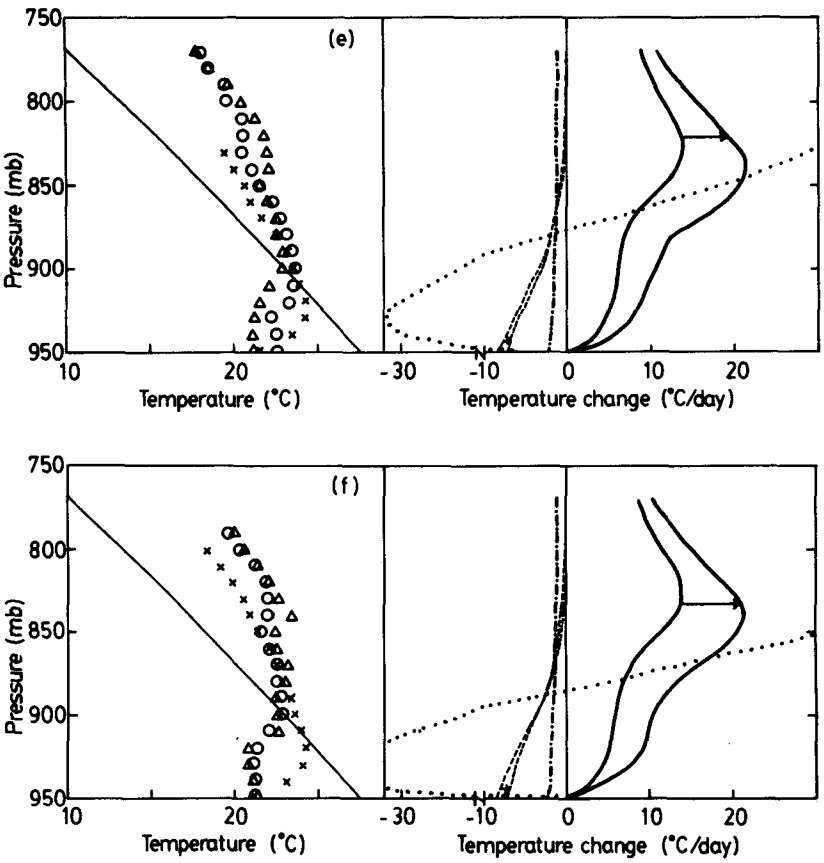

FIG. 9. (*Continued*)

Acknowledgments. The National Science Foundation (NSF) supported this research under Grants ATM-8210685, 8211842, and 8414371. The National Center for Atmospheric Research (sponsored by the National Science Foundation) provided the GMD rawinsonde tracking unit, balloons, helium, and the Airco sondes and ADAS computer system for analyzing the soundings. We thank Chuck Stearns for help with the ground flux sensors. Nick Wilde participated in the experiment at Canton, Oklahoma, as part of the rawinsonde team and spent long hours launching sondes, day and night. Special thanks also go to Robert McBeth for training the rawinsonde team, and for the tender loving care he gave to the GMD to keep it operating. The Corps of Engineers and state employees at Canton Reservoir Recreation Area provided logistic support, power, and the inflation shelter for the rawinsonde team; without their friendly cooperation this phase of the experiment could not have succeeded.

REFERENCES

André, J. C., and L. Mahrt, 1982: The nocturnal surface inversion and influence of clear-air radiative cooling. *J. Atmos. Sci.*, **39**, 864–878.

Estournel, C., R. Vehil and D. Guedalia, 1985: An observational study of radiative and turbulent cooling in the nocturnal boundary layer (ECLATS Experiment). *Bound.-Layer Meteor.*

Garratt, J. R., and R. A. Brost, 1981: Radiative cooling effects within and above the nocturnal boundary layer. *J. Atmos. Sci.*, **38**, 2730–2746.

Schaller, E., and M. Wichmann, 1985: Interaction of turbulent fluxes and mesoscale advection in the stably-stratified boundary layer. *Extended Abstracts: Seventh Symposium on Turbulence and Diffusion,* Boston, Amer. Meteor. Soc., 365–368.

Staley, D. O., and G. M. Jurica, 1970: Flux emissivity tables for water vapor, carbon dioxide and ozone. *J. Appl. Meteor.*, **9**, 365–373.

Stull, R. B., 1976: Mixed-layer depth model based on turbulent energetics. *J. Atmos. Sci.*, **33**, 1268–1278.

——, 1983a: A heat-flux-history length scale for the nocturnal boundary layer. *Tellus*, **35A**, 219–230.

——, 1983b: Integral scales for the nocturnal boundary layer. Part I: Empirical depth relationships. *J. Climate Appl. Meteor.*, **22**, 673–686.

——, 1983c: Integral scales for the nocturnal boundary layer. Part II: Heat budget, transport and energy implications. *J. Climate Appl. Meteor.*, **22**, 1932–1941.

——, and E. W. Eloranta, 1984: Boundary Layer Experiment—1983. *Bull. Amer. Meteor. Soc.*, **65**, 450–456.

Yamada, T., 1979: Prediction of the nocturnal surface inversion height. *J. Appl. Meteor.*, **18**, 526–531.

Zeman, O., 1979: Parameterization of the dynamics of stable boundary layers and nocturnal jets. *J. Atmos. Sci.*, **36**, 792–804.